Simulation of Laser-excited Surface Acoustic Waves Traveling on A Hemispherical Steel Shell

J. Mäkinen[1], D. Veira Canle[1], R. Blomqvist[1], A. Salmi[1*], E. Hæggström[1]
[1]Department of Physics, Division of Materials Physics, University of Helsinki, Helsinki, Finland
*Corresponding author: ari.salmi@helsinki.fi

Abstract

Non-contacting guided wave tomography based on laser ultrasonic waves permits inspecting structures that are inaccessible to traditional ultrasound methods. Such structures may be hard to reach, e.g. hot metal structures, metal implants inside tissue, and metals in chemically corroding environments. The shape of such structures is sometimes simple, which makes the propagation path of the guided waves well defined. A spherical structure requires that one accounts for multiple propagation paths and echoes of the guided waves. We set up a 3D multiphysics model in COMSOL Multiphysics® to verify our measurement results of guided wave propagation on a hemispherical steel shell featuring a Ø=9.5 mm hole.

The time dependent multiphysics model uses the Heat Transfer module to model the laser excitation as a heat source on the hemispherical steel shell. There are two mechanisms for guided wave generation by laser excitation: thermal expansion and ablation. Only thermal expansion was considered since the contribution from ablation is negligible at low excitation energies. The Heat Transfer module was coupled to the Structural Mechanics module to model generation of guided waves with the Thermal Expansion multiphysics coupling.

The predicted displacement on the outer rim of the hemispherical steel shell were compared to experimental results obtained with a system comprising an Nd:YAG laser excitation and a laser Doppler vibrometer (LDV) pickup. The simulated signals were first compared to measurement data for an intact hemispherical shell. Then to show the capability of damage detection, a simulation model of the hemispherical shell with a defect was analyzed.

Introduction

Guided acoustic waves (GAW) are a common way in industrial non-destructive evaluation (NDE) to assess the structural health of e.g. pipes, airplane parts, powerplant components, etc. [1-4]. The traditional way of exciting these waves is to use transducers that touch the object under inspection while measuring it with either another transducer or with a laser-based method [2,5-6]. For non-contacting evaluation, laser ultrasound provides a way to both create GAWs on a structure and to measure their propagation [1, 4, 6-10]. Guided waves are widely used on plate-like and tube-like structures. When tubular structures are concerned, the issue of multiple propagation paths arises [1, 9-10]. This is especially true when spherical geometries are considered. A specific case of spherical structures, a hemisphere, is even more challenging due to multiple propagation paths along the isocircles combined with the interference from wall echoes at the measurement point. This also makes defect detection and localization challenging.

In this paper, we tackle the problem of guided wave NDE on two nearly identical hemispheres by creating two models in COMSOL Multiphysics®: one to compare the signals on a flawless hemispherical shell and one to do the same on a shell with a defect.

Theory

Propagating GAWs, more specifically Lamb waves, feature two fundamental mode families that can be detected, the symmetric and antisymmetric modes [11-13]. Most acoustic power is in the two lowest order waves: the symmetric mode (S_0) and the antisymmetric mode (A_0).

To generate Lamb waves, we used laser excitation. There are two mechanisms, or regimes, that generate ultrasonic waves [4]: ablation at high and thermoelastic at low energy densities. To perform non-destructive excitation the energy density of the laser must be sufficiently low so that no ablation occurs, but sufficiently high that the localized heating generates sufficient thermoelastic stress (thermoelastic regime). The simulation model is built assuming that we employ thermoelastic excitation.

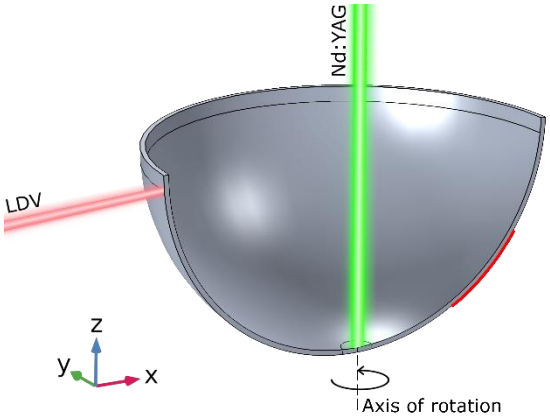

Figure 1: Schematic picture of a hemispherical shell and positions of laser spots. Nd:YAG excitation at the zenith on the inner surface of the hemispherical shell and LDV pick-up on the outer rim at 1.85 mm distance from the edge. The red line specifies the area used for the dispersion curves in Fig. 6.

Experimental Set-up

The experiments were conducted for a hemispherical steel shell that was attached to a 3D-printed holder made of PLA. The holder allowed the hemispherical shell to be azimuthally rotated around a fixed axis for a 360° measurement. A CFR Big Sky Laser Series pulsed Q-switched Nd:YAG laser (1064 nm wavelength, 8 ns pulse length,40 mJ pulse energy and Ø=1 mm full width at half maximum) was used to excite the GAWs at the inner, zenith point of the hemispherical shell. A Polytec OFV-303 laser Doppler vibrometer (2 MHz bandwidth) detected the propagation of the launched GAWs on the outer rim of the hemispherical shell, at 1.85 mm distance from the top of the structure. The spot size of the LDV was 33 µm. Measurements were done normal to the outer surface of the shell. A schematic of the hemispherical shell and the positions of the contacting points with the lasers beams are shown in Fig 1.

Simulation Model

In COMSOL Multiphysics® v5.3a the Solid Mechanics Module and the Heat Transfer Module were combined using the built-in multiphysics coupling for thermal expansion. This coupling was used to model the time dependent generation of elastic waves through rapid thermal expansion in a hemispherical steel shell.

The outer diameter of the modeled hemispherical shell was 50.3 mm and the wall thickness was 0.6 mm. Material properties for steel were obtained from the material library provided in COMSOL. The material parameters used are shown in Table 1.

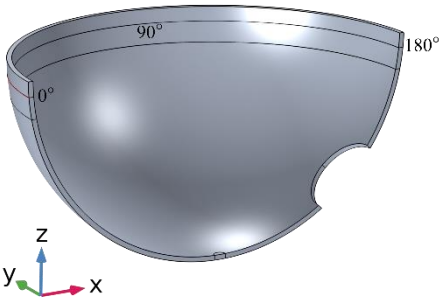

Figure 2: Geometry of the 3D model using symmetry in y-direction. A circular defect with a radius of 9.5 mm is added compared to Fig 1. The angles shown correspond to the measurement direction in Fig 6.

A 2D axisymmetric model was first used to test and compare the model against measurements for an intact hemispherical shell, Fig. 1. Then a model featuring a defect, a Ø=9.5 mm hole, was modeled in 3D, Fig. 2. To reduce the size of the simulation domain, the defect was selected as a hole which reduced the domain by half.

To model the heating from a laser source, a Boundary Heat Source was used. According to [4] the power of a laser beam on a metal surface is absorbed within a few nanometers thick layer so a boundary source was chosen, and the depth profile of the absorption was neglected. Equation (1) was used to model the laser beam profile:

$$Q(x,y,t) = E(1-R)f(x)f(y)g(t) \qquad (1)$$

$$f(r) = \frac{1}{\sigma_r\sqrt{2\pi}} e^{-\frac{r^2}{2\sigma_r^2}}, \quad \sigma_r = \frac{w}{2\sqrt{2ln2}} \qquad (2)$$

$$g(t) = \frac{1}{\sigma_t\sqrt{2\pi}} e^{-\frac{(t_{ex}-t)^2}{2\sigma_t^2}}, \quad \sigma_t = \frac{t_{ex}}{4} \qquad (3)$$

The first parameters in Eq. (1) describes the energy of the laser beam transferred to the solid. *E* is the energy of the laser pulse and *R* is the reflectance of polished steel [4]. *f(r)* describes the spatial, gaussian shape of the laser beam [4], where *w* is the FWHM of the beam. *g(t)* is a gaussian modulation of the beam in time to smoothen the input for numerical purposes. t_{ex} is the duration of the laser pulse. Numerical values and descriptions of the parameters are shown in Table 1.

For cooling of the metal, the emissivity ε of the surface was model as a Diffuse Surface boundary,

though its effect was small. Convective cooling was insignificant at the simulated time scale.

Since the simulation considers wave propagation, the CFL condition was imposed for the time stepping δt scheme and an appropriately sized mesh h was used [15]:

$$\delta t = \frac{CFL * h}{c}, CFL = 0.2$$
$$h = \frac{\lambda}{8} = \frac{c_l}{8f}$$

For the frequency f, a convergence study was run in the expected range of low MHz for the higher frequency Lamb wave modes. Beyond 2 MHz, the solutions didn't change significantly. Related to the CFL condition, the discretization of the mesh was set as Quadratic Lagrange and the solver used the generalized-α method. Since the duration of the laser pulse was 8 ns, the simulation was run with a shorter time stepping scheme in the beginning to properly consider the laser beam's duration. The mesh was refined around the heated area.

Parameter	Symbol	Value	Source
Coefficient of thermal expansion	α	$12.3*10^{-6}$ 1/K	*
Heat capacity at constant pressure	C_p	475 J/(kg*K)	*
Thermal conductivity	k	44.5 W/(m*K)	*
Density	ρ	7850 kg/m^3	*
Poisson's ratio	ν	0.28	*
Young's modulus	Y	205 GPa	*
Longitudinal speed of sound	c_l	5778 m/s	*
Beam energy	E	40 mJ	
Reflectance	R	0.63	[4]
Beam width	w	1 mm	
Pulse length	t_{ex}	8 ns	
Surface emissivity	ε	0.7	[14]

Table 1: Parameters used in the simulations, *material data from COMSOL's material library for steel AISI 4340

Results and Discussion

Simulation results for the 2D axisymmetric model are presented in Fig. 3. Here the normal displacement at the inner and outer surfaces is plotted at a point 1.85 mm below the edge of the hemispherical shell (Fig. 1, LDV position) from 5 µs to 15 µs. At 7 µs the first wave arrives at the measurement point. The displacement of the wave is symmetrical, corresponding to the first symmetric Lamb wave mode (S_0). After 11 µs, an antisymmetric wave package with a greater amplitude arrives. The effect of the waves reflecting off the edges of the shell is seen in the peaks at ~12µs. This indicates that the signal depends on the

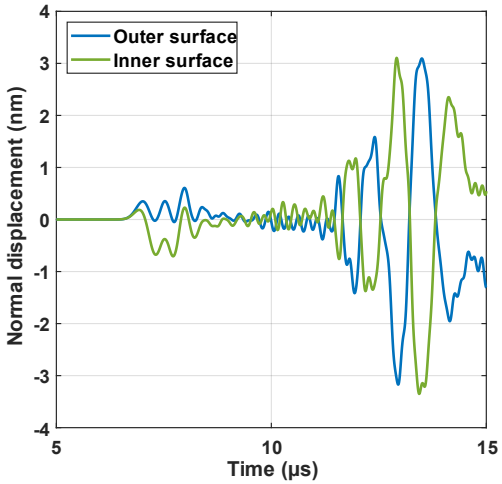

Figure 3: 2D axisymmetric simulation wave amplitude normal to the surface at 1.85 mm distance from the edge of the hemispherical shell on both the inner (green) and outer (blue) surface.

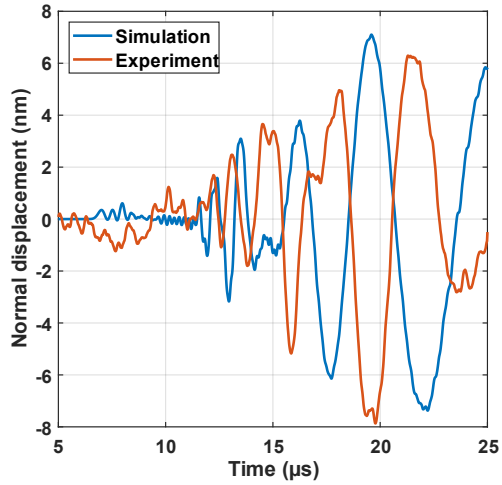

Figure 4: Wave amplitude normal to the surface. Simulation (blue) compared to experiment (orange) determined at 1.85 mm distance from the edge of the hemispherical shell.

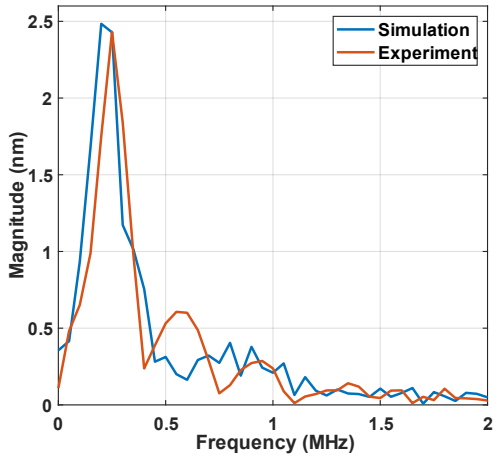

Figure 5: Frequency spectrum of the measured and simulated signals in Figure 4.

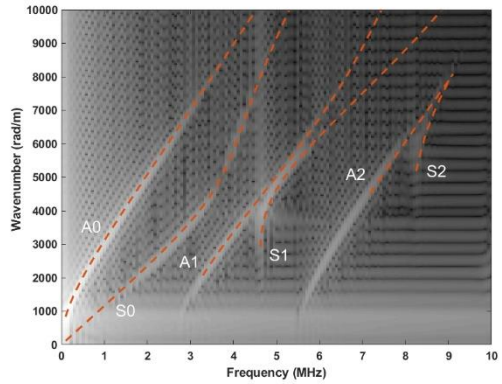

Figure 6: Dispersion curves of the 2D axisymmetric simulation. Theoretical predictions for six Lamb wave modes are plotted with orange lines.

measurement point coordinate, the hemispherical shell's edge topology, and the shape of the incoming wave beyond the 12 µs mark.

Comparing simulation data to a 25µs long experiment exemplifies this. In Fig. 4 one sees that the general shape of the signals is similar, but the further we go in time the more the signals appear to get out of phase. The symmetric Lamb wave mode at 7 µs is not visible in the measured signal.

To further compare the experimental and simulated data in Fig. 4, the frequency contents of both signals were determined. The Fourier transform of the signals is presented in Fig. 5. There is an amplitude maximum at 250 kHz in both signals. Three frequency peaks are seen in the measured signal while only two clear peaks are visible in the simulation.

The Lamb wave modes present in the simulation were examined by plotting the dispersion curve along the outer edge of the hemispherical (edge depicted as a red line in Fig. 1). The time scale was limited from 0 to 12.6 µs. In Fig. 6 the 2D Fourier transform is plotted and theoretical Lamb wave modes for a plate of the same thickness were calculated with The LAMB toolbox, MATLAB® (version R2018a) [16]. The Lamb wave modes obtained from the simulation data match the theoretical values. Theoretical modes were phase speed limited to 9100 m/s. We also realize why the S_0 mode is hard to see in the measured data. The LDV bandwidth was 2 MHz, thus most of the S_0 band is outside the measurement band.

Figure 3 shows that to detect a defect in the measured signal, we should focus on the antisymmetric modes arriving after 11 µs. A defect should also be visible in a simulation by looking at the symmetric modes arriving at 7 µs, but not in a measurement. If there is a defect on the propagation path of a wave, the wave is reflected and scattered. Hence a defect should be detectable from the

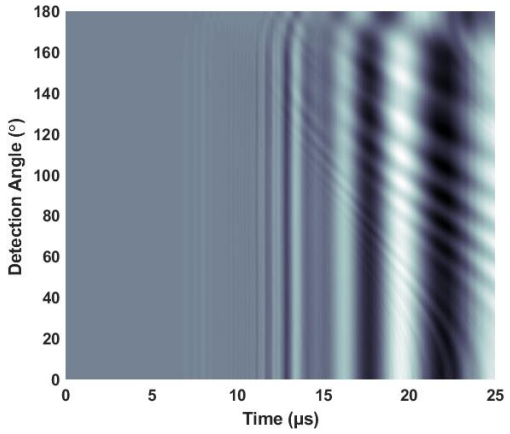

Figure 7: Waterfall plot of the hemispherical shell in Fig 2. On the y axis is the measurement position along the rim at 1.85 mm from the edge of the structure. The color scale indicates the amplitude of the signal.

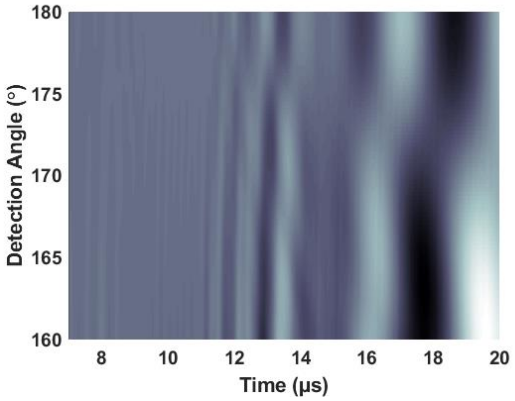

Figure 8: Zoom in into Fig. 7 shows the trace of the defect.

measured signal by comparing it to signals from the part of the hemispherical shell with no defect. This can be done in our set-up by rotating the shell around the axis (Fig. 1) and by mapping the displacement field along the rim.

The displacement plots (similar to Fig. 4) for the 3D model with a defect (Fig. 2) are plotted as a waterfall plot in Figs. 7-8. The y-axis represents the azimuthal angle from 0° to 180° marked in Fig.4. These images show the impact of the defect on the antisymmetric modes at 180°. In Fig. 7 the reflections from the defect can be seen by looking at the disturbances in the amplitudes after 12 µs.

Conclusions

We showed that COMSOL Multiphysics® can model the thermoelastic structural interaction that produces Lamb waves on a hemispherical structure produced with laser ultrasonic excitation. Measured results for a 0.6 mm thick hemispherical shell were compared to those predicted by simulations. The simulated data shows that a defect should be detectable experimentally.

References

1. J.-H. Lee, S.-J. Lee, Application of laser-generated guided wave for evaluation of corrosion in carbon steel pipe, *NDT&E International*, **42**, 222-227 (2009)
2. R. P. Dalton et al., The Potential of Guided Waves for Monitoring Large Areas of Metallic Aircraft Fuselage Structure, *Journal of Nondestructive Evaluation*, **20**, 29-46 (2001)
3. T. Tanaka and Y. Izawa, Nondestructive Detection of Small Internal Defects in Carbon Steel by Laser Ultrasonics, *Jpn. J. Appl. Phys.*, **40**, 1477-1481 (2001)
4. C. B. Scruby and L. E. Drain, *Laser Ultrasonics Techniques and Applications*, Taylor & Francis Group, New York (1990)
5. W. J. Stashzewisk et al., Structural health monitoring using scanning laser vibrometry: I. Lamb wave sensing, *Smart Mater. Struct.*, **13**, 251-260 (2004)
6. N. David, The Interaction of Lamb Waves with Defects, *IEEE UFFC*, **39**, 381-397 (1992)
7. R. E. Green Jr., Non-contact ultrasonic techniques, *Ultrasonics*, **42**, 9-16 (2004)
8. W. Gao et al., Laser ultrasonic study of Lamb waves: determination of the thickness and velocities of a thin plate, *International Journal of Engineering Science*, **41**, 219-228 (2003)
9. D. Clorennec et al., Nondestructive evaluation of cylindrical parts using laser ultrasonics, *Ultrasonics* **40**, 783-789 (2002)
10. D. Clorennec et al., Analysis of surface acoustic wave propagation on a cylinder using laser ultrasonics, *Appl. Phys. Lett.*, **82**, 4608 (2003)
11. H. Lamb, On Waves in an Elastic Plate, *Proc. R. Soc. A*, **93**, 114-128 (1917)
12. D. N. Alleyne and P. Cawley, Optimization of Lamb wave inspection techniques, *NDT & E International*, **25**, 11-22 (1992)
13. B. C. Lee and W. J. Staszewski, Modelling of Lamb waves for damage detection in metallic structures: Part I. Wave propagation, *smart Mater. Struct*., **12**, 804-814 (2003)
14. R. Fakir et al., Case study of laser hardening process applied to 4340 steel cylindrical specimens using simulation and experimental validation, *Case Studies in Thermal Engineering*, **11**, 15-25 (2018)
15. COMSOL® Multiphysics, Acoustics Module User's Guide, version 5.3a, 153-154 (2017);
16. J. L. Prego, The LAMB toolbox (https://se.mathworks.com/matlabcentral/fileexchange/28367-the-lamb-toolbox), MATLAB Central File Exchanger, Retrieved September 26, 2018